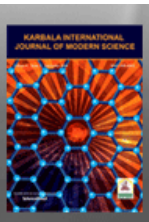
Karbala International Journal of Modern Science

Manuscript 3328

Optical, Structural, and Electrochemical Properties of P3HT:Y6 Photoactive Layer for Organic Photovoltaics

Hassan Tarikhum B.

Furqan Almyahi

Basil Ali

Optical, Structural, and Electrochemical Properties of P3HT:Y6 Photoactive Layer for Organic Photovoltaics

Abstract

Recently, organic photovoltaics (OPV) have emerged as a promising technology for environmentally friendly energy production. Achieving high performance in OPV requires the discovery of novel compounds. This article aims to study the optical, structural, electrochemical, and electrical properties of a P3HT:Y6 blend. The UV-visible spectra of the blend provided insight into how composition affects the optoelectronic properties of OPV devices. The optimised P3HT:Y6 ratio (0.6:1) resulted in the largest redshift and the highest absorption intensity. Raman and X-ray diffraction tests showed low aggregation and low crystallinity of the polymer P3HT as Y6 content increased. In the OPV devices, the best performance was recorded at a 0.6:1 ratio, with an effi-ciency of 2.84%.

Keywords

poly (3-hexylthiophene) (P3HT); non-fullerene acceptor (NFA); organic photovoltaics (OPV); Raman spectrum; cyclic voltammetry (CV)

RESEARCH PAPER

Optical, Structural, and Electrochemical Properties of P3HT:Y6 Photoactive Layer for Organic Photovoltaics

Hassan Tarikhum B. [a,b,*], Furqan Almyahi [b], Basil Ali [b]

[a] Department of Physics, College of Science, Al-Muthanna University, Samawa, Iraq
[b] Department of Physics, College of Science, University of Basrah, Basrah, Iraq

Abstract

Recently, organic photovoltaics (OPV) have emerged as a promising technology for environmentally friendly energy production. Achieving high performance in OPV requires the discovery of novel compounds. This article aims to study the optical, structural, electrochemical, and electrical properties of a P3HT:Y6 blend. The UV-visible spectra of the blend provided insight into how composition affects the optoelectronic properties of OPV devices. The optimised P3HT:Y6 ratio (0.6:1) resulted in the largest redshift and the highest absorption intensity. Raman and X-ray diffraction tests showed low aggregation and low crystallinity of the polymer P3HT as Y6 content increased. In the OPV devices, the best performance was recorded at a 0.6:1 ratio, with an efficiency of 2.84%.

Keywords: Poly(3-hexylthiophene) (P3HT), Organic photovoltaics (OPV), Non-fullerene acceptor (NFA), Cyclic voltammetry (CV)

1. Introduction

Utilising organic materials has greatly increased the effectiveness of OPV over the past few years, especially since the development of advanced materials known as non-fullerene small-molecule acceptors, such as the Y6 molecule, which can harvest photons in the near-infrared (NIR) region because of their adjustable energy levels and facilitate appropriate exciton dissociation and charge transport [1–3]. To produce highly efficient OPVs, suitable conjugated polymer structures that absorb the maximum number of photons must be designed [4]. The binary approach, wherein a non-fullerene acceptor is combined with a donor polymer in a single-layer bulk heterojunction (BHJ) device, can further boost the power conversion efficiency (PCE) of polymers [5]. P3HT-based photovoltaic cells using effective non-fullerene small-molecule acceptors achieved an open-circuit voltage (V_{OC}) of 1.02 V and a PCE of 11.27% [6,7]. A novel OPV with over 15% efficiency was synthesised in 2019 by Fan et al. [8], who used a series of benzotriazole (TzBI)-based donors mixed with Y6 as an acceptor material. In 2020 [9], a PTzBI-dF:Y6 device achieved a high PCE of 16.7%. Ding et al. [10] developed a groundbreaking copolymer named D16 in 2019. Its unique composition (the thiolactone unit and its derivatives) has increased in π−π stacking and high hole mobility. This copolymer donor significantly boosted the efficiency of OPV by up to 16.72%. A 2020 study [11] showed that using a fused-ring acceptor unit in the copolymer donor D18 increases efficiency. This effect is evidenced by the fact that solar cells based on D18:Y6 achieved a PCE of 18.22%, marking a significant milestone in which binary OPV devices achieved a PCE of over 18% for the first time. Utilising the polymer P3HT combined with the non-fullerene acceptors Y6, Y5, and TPBT-RCN as photoactive layers was studied by Yang et al. [12]. The P3HT-based OPVs at 140 °C exhibited the best PCE of 2.41% with Y6. Due to their suitable energy levels and high open circuit voltage, TPBT-RCN-based devices outperformed those based on Y6 and Y5 and achieved a PCE of 5.11%.

Received 30 June 2023; revised 24 August 2023; accepted 28 August 2023.
Available online 12 October 2023

* Corresponding author at: Department of Physics, College of Science, Al-Muthanna University, Samawa, Iraq.
E-mail address: hassan.tarikhum@mu.edu.iq (H. Tarikhum B.).

https://doi.org/10.33640/2405-609X.3328

In our study, we prepared a P3HT:Y6 blend at different weight ratios as a photoactive layer for OPV devices. The blend was prepared using a co-solvent of chloroform (CF) and chlorobenzene (CB) in a 70:30 ratio with a 20 mg/mL concentration. Using thin films and dilute solutions, we meticulously examined the photoactive layers' optical, structural, and electrochemical properties. The photovoltaic properties were measured under ambient conditions with devices constructed with ITO/PEDOT-PSS/P3HT:Y6/ZnO/Al structures with an area of 0.06 cm^2. The main parameters of OPV devices were calculated. The devices attained a maximum power conversion efficiency of 2.84%.

2. Material and methods

2.1. Materials

Poly(3-hexylthiophene) (P3HT) with 20 kg/mol molecular weight (Mn) was synthesised according to the literature [13]. A non-fullerene acceptor, Y6, was purchased from 1-Material Company. While the Poly(3,4-ethylene dioxythiophene)-poly(styrene sulfonate) (PEDOT-PSS) was acquired from Ossila. ZnO nanoparticles were synthesised in the laboratory according to the literature [14]. Indium tin oxide (ITO) anode electrodes with a 3*15 mm^2 area and 8–10 Ω cm^{-2} sheet resistance were procured from China. The organic solvents were procured from Sigma–Aldrich. Finally, commercially available Al wire was used as the cathode electrode.

2.2. Thin film and device manufacturing

The OPV device preparation and fabrication processes were carried out according to the literature [15]. At a 20 mg/mL concentration, P3HT:Y6 blends with various weight ratios (1:0, 1:0.6, 1:0.8, 1:1, 0.8:1, 0.6:1, 0.4:1, and 0:1) were prepared and dissolved in 1 mL of CF:CB (70:30) solvent. The blends were stirred for 2 h. Quartz and glass-ITO substrates were meticulously cleaned by using deionized water, acetone, and isopropyl alcohol through ultrasonic cleaning. Then they were subjected to a UV-ozone environment for 20 min after being dried at 100 °C for 15 min. To examine the physical properties, P3HT:Y6 thin films in different weight ratios were spin-coated at 2000 rpm for 1 min on quartz substrates. Finally, the samples were annealed for 5 min at 140 °C.

The following procedures were performed to manufacture OPV: First, as hole transport layers, the PEDOT-PSS layers were spin-coated at 4000 rpm for 1 min on cleaned ITO substrates. Subsequently, the thin layers were allowed to dry for 20 min at 140 °C. Second, the P3HT:Y6 photoactive layers were spin-coated on top of the PEDOT-PSS layers at 2000 rpm for 1 min. Third, as electron transport layers, the ZnO nanoparticle layers were coated for 1 min at 4000 rpm. After that, the samples were annealed for 5 min at 140 °C. Finally, Al layers were deposited as cathode electrodes for OPV devices.

2.3. Characterisation techniques

In order to determine the absorption curves of the dilute solutions and solid-state thin films, we used a visible-NIR spectrometer (Shimadzu UV-1800 PC). A wavelength range of 300–900 nm was used for the solutions, whereas a wavelength range of 300–1100 nm was used for the solid-state thin films. With an excited wavelength of 532 nm, a JD-785-300 mW laser was used to acquire the Raman spectra. Using angles ranging from 2° to 40°, an X-Pert diffractometer was used to obtain the X-ray spectra. With a Corr-Test electrochemical workstation, the cyclic voltammetry measurements were carried out using a working electrode (a Pt plate), a counter electrode (a Pt wire), and a reference electrode (a standard calomel electrode), all dipped in 0.1 M tetrabutylammonium hexafluorophosphate (Bu4NPF6) acetonitrile solution as electrolyte. A Keithley source meter 2400 (SCIENCE TECH) and solar simulator lamp AM1.5 systems with illumination of 100 mW/cm^2 were used to measure current–voltage on the OPV devices.

3. Results and discussion

3.1. Optical properties

Fig. 1(a) displays the absorption spectra of the P3HT thin films prepared using various solvents. Moreover, Fig. 1(b) exhibits the normalised spectra of the Y6 thin films. CB, CF, CF:CB (50:50), and CF:CB (70:30) solvents were used to determine the optimal solvent for Y6 and P3HT materials. In a 70:30 co-solvent ratio, Y6 and P3HT displayed the highest intensity and redshift among the solvents. Notably, the distinct peaks in the P3HT spectrum signified the polymer's self-assembly. To determine the best concentration of the P3HT:Y6 blend, we prepared binary thin films with a 1:1 ratio and dissolved them in CF:CB (70:30) at 10, 20, 30, and 40 mg/mL concentrations. Fig. 1(c) displayed a significant increase in absorption intensity in the polymer area of the spectrum when a 20 mg/mL concentration was used. A low concentration seemed to lead to an increase in polymer chain aggregates.

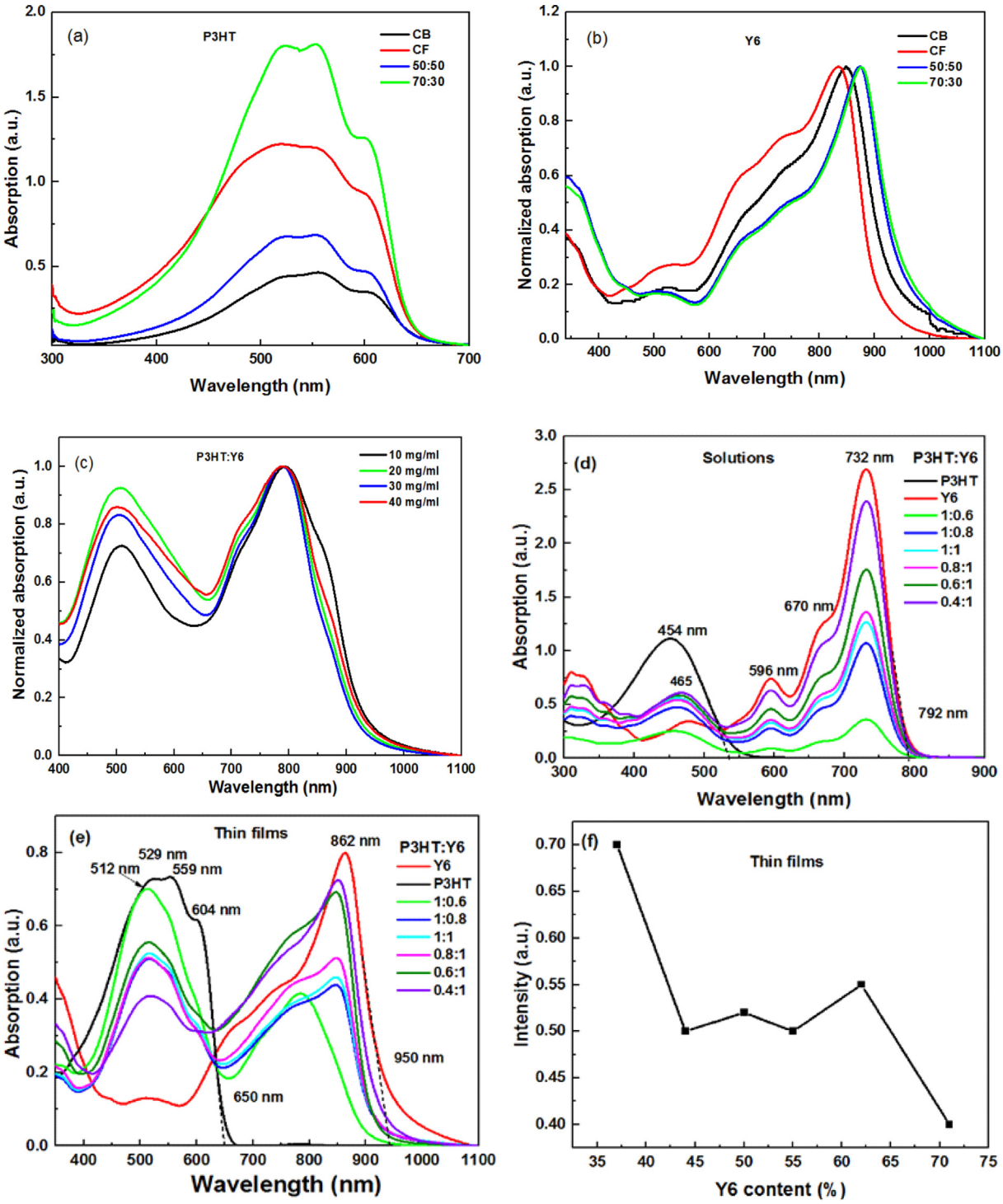

Fig. 1. Absorption spectra as a function of different solvents of (a) P3HT, (b) Y6 solid-state thin films, and (c) as a function of different concentrations of P3HT:Y6 thin films. (d) the absorption spectra of P3HT-based blends with different ratios of Y6 at a concentration of 20 mg/mL and CF:CB (70:30) solvent as dilute solutions and (e) as thin films, while (f) shows the impact of the change in absorption intensities using the CF:CB (70:30) co-solvent for the blend of P3HT:Y6.

Fig. 1(d) shows the absorption spectra of the P3HT:Y6 blend dilute solution. At a concentration of 20 mg/mL, a P3HT:Y6 blend with different weight ratios was prepared and dissolved in 1 mL of CF:CB (70:30) solvent. Y6's absorption featured an absorption edge onset at 792 nm, which matched an optical energy gap (*Eg*) of 1.56 eV, with a main peak at 732 nm, 596 nm, and 670 nm. Moreover, the

P3HT:Y6 spectra showed high absorption intensity at 454 nm, attributed to polymer absorption On the other hand, the thin films exhibited broader absorption spectra and more growth and redshifts than the dilute solutions, as depicted in Fig. 1(e). Indicated the self-organisation of molecules, aggregation of the molecular backbone, and $\pi-\pi^*$ interactions [16,17]. The Y6 thin film's spectrum showed a strong intensity at 862 nm, with the absorption edge onset at 950 nm and an *Eg* of 1.3 eV. The P3HT thin film, on the other hand, exhibited substantial visible-range absorption, with an absorption edge onset at 650 nm matching an energy gap of 1.9 eV. Moreover, it displays a maximum absorption peak of 559 nm, 529 nm, and 604 nm, corresponding to 0–1, 0–2, and 0-0 transitions, respectively [18]. On the other hand, the P3HT:Y6 thin films have absorption spectra that range from 400 nm to 950 nm, with the main peak at 512 nm, which corresponds to a 0–2 transition and suggests that polymer chains had a new rearrangement [19]. Therefore, the blend ratio can modify molecule stacking behaviour [20]. Fig. 1(f) shows the impact of the change in absorption intensities of the P3HT:Y6 blend thin films as a function of the content of Y6 caused by using the CF:CB (70:30) co-solvent. At 72%, there is a sharp drop in intensity, attributed to a drop in the P3HT crystallinity during film growth. The *Eg* values were estimated by intersecting the x-coordinate with the tangent line of the absorption edge [21]. These values were compared with those estimated using Tauc's equation given by [22]:

$$\alpha h\nu = A(h\nu - Eg)^m \quad (1)$$

The parameter '*m*' is connected to the nature of electron transitions and is 1/2 for direct transitions [23]. α refers to the absorption coefficient, *A* represents absorption intensity, and hν is the incident photon's energy. Fig. 2(a) and (b) show a relationship between $(\alpha h\nu)^2$ and $(h\nu)$ for dilute solutions and thin films, respectively. The thickness of thin films is approximately 125 nm, while the thickness of the dilute solution is 1 cm. The insets describe the intersection between the tangent line at absorption edge onset and the x-axes for the energy gap estimate. The optical energy gap values obtained from both methods are similar, as shown in Table 1.

3.2. Structural properties

Raman spectroscopy was employed to examine the crystallinity of the utilized materials during thin film growth, with an excitation wavelength of 532 nm. Fig. 3(a) and (b) show the Raman spectra of neat P3HT and Y6 films, respectively. Fig. 3(c) displays the Raman spectra of the P3HT:Y6 thin films. The Raman spectra of the blended thin films exhibited similarities to the spectra of the P3HT films. Notably, the Raman spectra were characterised by main modes at 1392 cm^{-1} and 1464 cm^{-1}

Table 1. Optical energy gap (Eg) values of binry blend, which were estimeted using Tauc and onset methods.

P3HT:Y6 blend wt%	Solid-state thin films		Dilute solutions	
	Eg onset (eV)	*Eg Tauc (eV)*	*Eg onset (eV)*	*Eg Tauc (eV)*
1:0	1.9	1.9	2.3	2.29
1:0.6	1.38	1.39	1.59	1.59
1:0.8	1.36	1.33	1.59	1.56
1:1	1.35	1.32	1.58	1.56
0.8:1	1.35	1.31	1.58	1.55
0.6:1	1.35	1.30	1.58	1.55
0.4:1	1.34	1.29	1.57	1.54
0:1	1.3	1.28	1.56	1.54

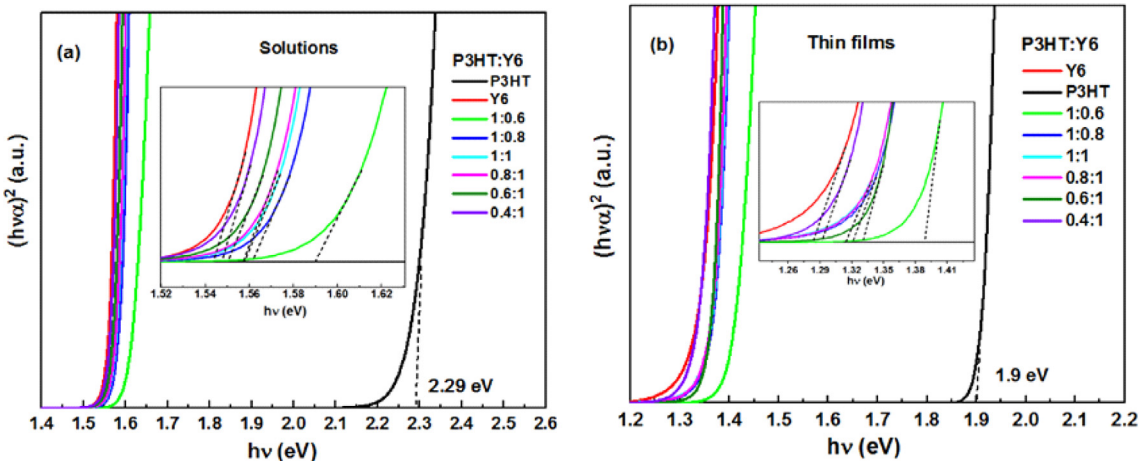

Fig. 2. Tauc plots of P3HT-based blends with various ratios of Y6 (a) in the case of dilute solutions and (b) in the case of solid-state thin films.

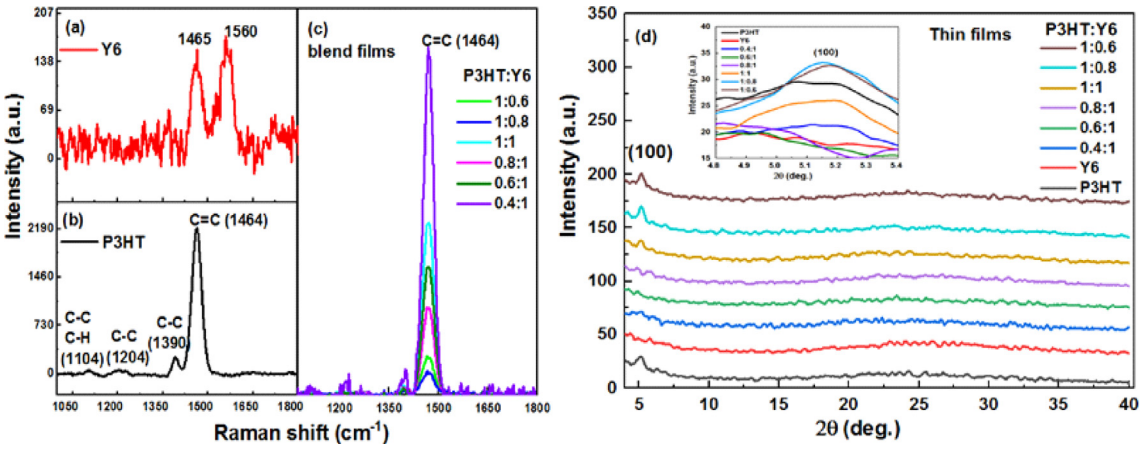

Fig. 3. Raman spectra of (a) pure P3HT, (b) pure Y6 films, (c) P3HT:Y6 blend thin films, and (d) XRD patterns of P3HT:Y6 films. The inset shows the peak at 2θ = 5.2 arising from P3HT (100).

positions, which indicate the C−C and C=C symmetric modes, respectively, which are characteristic in Raman's pattern of P3HT. In addition, two minor peaks manifested at 1104 cm^{-1} and 1204 cm^{-1} [24]. For Y6, the Raman spectra displayed two regions of vibration that exhibited relatively high intensities. These regions were located at 1560 and 1465 cm^{-1}, attributed to the alkene and thiophene vibrations, respectively [25]. The relative intensity ($I_{C=C}/I_{C-C}$) provides insight into the conformation of the backbone and molecular organisation of P3HT chains within a solid-state thin film [24]. An increase in planarity and aggregation of polymer chains is determined by the $I_{C=C}/I_{C-C}$ ratio [26]. Small $I_{C=C}/I_{C-C}$ values clearly indicate a high level of conformation and increased aggregation. Conversely, large $I_{C=C}/I_{C-C}$ values referred to a more twisted [27]. In Table 2, a decrease in the $I_{C=C}/I_C$ with a decrease in Y6 content (1:0.6 and 1:0.8 ratios) can be attributed to an increase in the planarity of the polymer. At the same time, we observed an increase in the relative intensity with ratios of 1:1, 0.8:1, 0.6:1, and 0.4:1, which attribute to a decrease in the planarity of film chains and, thus, more decreased aggregation. As a result, a drop in relative intensity values can be correlated with an increase in the π-electron density within C−C bonds, which is brought on by an increase in the planarity of the polymer chains [27].

To survey the packing of the thin films, X-ray diffraction (XRD) was used. The XRD spectra of the P3HT:Y6 thin films are depicted in Fig. 3(d), displaying the diffraction peak of P3HT due to the π−π stacking of backbones at 2θ = 5.2, which corresponds to diffraction from the (100) plane [28]. The XRD parameter values, which corresponded to peak positions at 2θ = 5.2, are shown in Table 3. The results indicated that the impact of adding Y6 to the blend became apparent as the peak in the 0.4:1, 0.6:1, and 0.8:1 samples disappeared, indicating a decrease in crystallinity because Y6 is a non-fullerene small molecule without a high molecular order. At 2θ ≈ 5.2, the (100) d-spacing values were estimated using Bragg's law [29]. The decrease in d-spacing of P3HT:Y6 thin films as content Y6 increases is shown in Table 3. The reduced spacing in the blend samples, in particular the 0.4:1, 0.6:1, and 0.8:1, indicates a disordering of the polymer chains during film growth [30].

Table 2. Obtained parameters using the Raman shift of P3HT:Y6 thin films.

P3HT:Y6 blend wt%	Solid-state thin films			
	Height C=C (cts)	*Height C−C (cts)*	$I_{C=C}/I_{C-C}$	FWHM (cm^{-1})
1:0	2193	249	8.8	38.39
1:0.6	392	48	8	41.9
1:0.8	244	48	5	43.44
1:1	1770	96	18.4	41.02
0.8:1	903	78	11.5	40.88
0.6:1	1325	68	19	41
0.4:1	3617	276	13	37

Table 3. Obtained parameters using the XRD patterns of P3HT:Y6 thin films.

P3HT:Y6 blend wt%	Solid-state thin films			
	Pos.[°2Th.]	*Height (100) (cts)*	*d-spacing (Å)*	FWHM (°2Th.)
1:0	5.04	20.58	17.52	0.47
1:0.6	5.13	23.59	17.22	0.62
1:0.8	5.19	26.49	17.00	0.27
1:1	5.08	19.93	17.39	0.94
0.8:1	–	–	–	–
0.6:1	–	–	–	–
0.4:1	–	–	–	–

3.3. Electrochemical properties

The cycle voltammetry curves for the thin films were measured against the potential of SCE a 20 mV/s scan rate, as shown in Fig. 4. During a positive potential sweep, the forward scan is called the oxidative potential or anodic direction. This scan resulted in the emergence of a peak called the anodic peak.

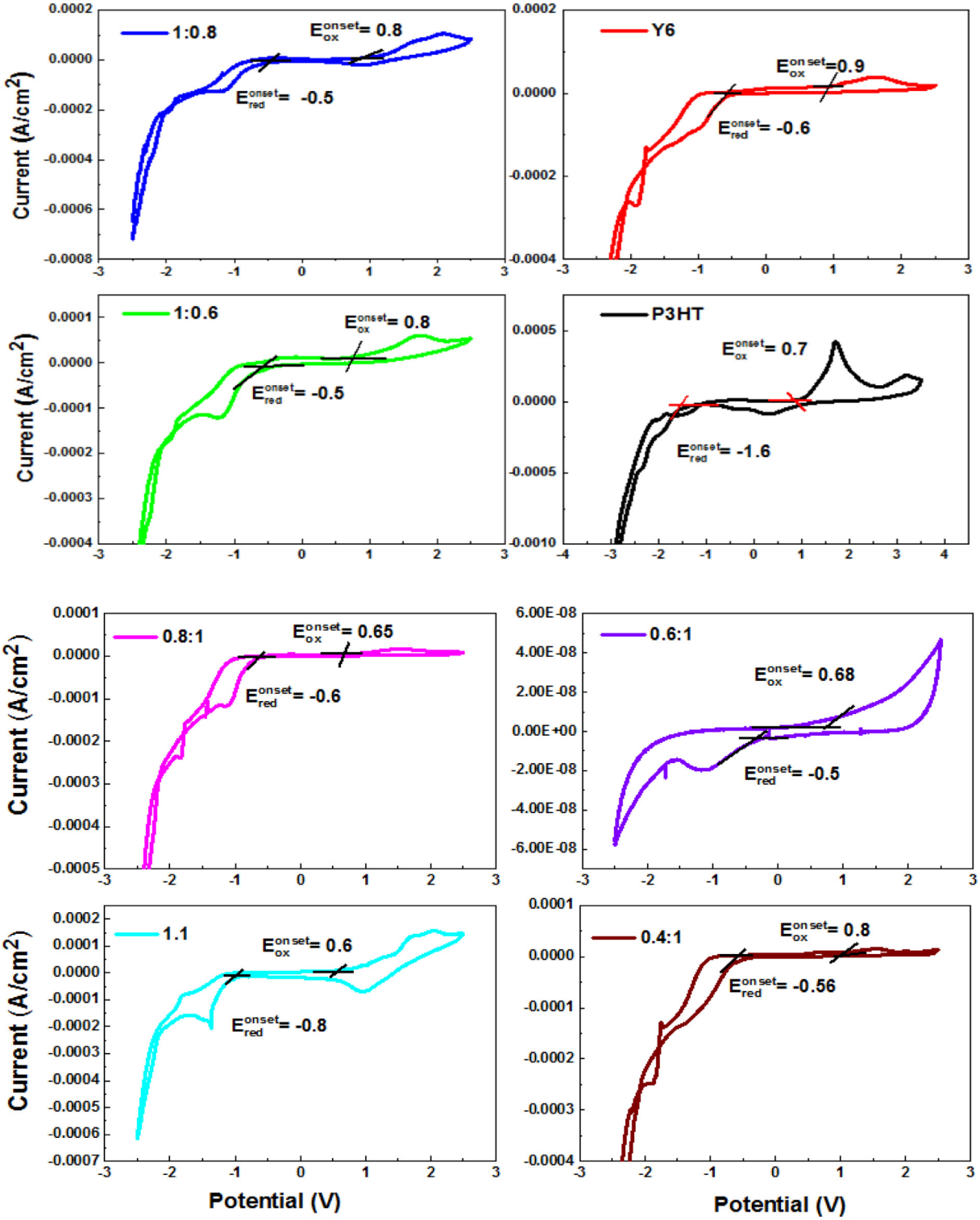

Fig. 4. Cyclic voltammetry spectra of P3HT:Y6 blends. The cross-dash lines were used to estimate the positions of oxidation (E_{ox}) and reduction (E_{red}) potentials.

Conversely, when the scan direction was reversed, the negative sweep of the reductive potential, referred to as the cathodic direction, produced a cathodic peak. The highest occupied molecular orbital (HOMO) and lowest unoccupied molecular orbital (LUMO) energy levels in eV units of the thin films were calculated according to the following equations [31]:

$$E_{HOMO} = -e(E_{ox} + 4.8) \quad (2)$$

$$E_{LUMO} = -e(E_{red} + 4.8) \quad (3)$$

where the E_{ox} and E_{red} represent the onset of oxidation and reduction potentials, respectively. 4.8 is the absolute energy level [32]. Thus, the Eg values were estimated according to the following equation [33]:

$$Eg = E_{LUMO} - E_{HOMO} \quad (4)$$

The electrochemical parameters of the P3HT-based blends at various weight ratios of Y6 are summarised in Table 4. The energy levels (E_{HOMO}/E_{LUMO}) of P3HT and Y6 obtained were −5.5/−3.2 and −5.7/−4.2, respectively. Moreover, the energy levels of blends were compatible with those of pure materials. Fig. 5 depicts the energy levels diagram of the OPV layers. The HOMO and LUMO level values of PEDOT-PSS, ZnO, Al, and ITO layers were based on the literature [34].

3.4. Electrical properties

The electrical properties of OPV devices were estimated by the manufacture of conventional solar cells according to the construction of ITO/PEDOT-PSS/P3HT:Y6/ZnO/Al with an area of 0.06 cm^2. Prior to conducting the measurements, the solar cells were annealed at a temperature of 140 °C, which was investigated promptly to prevent the oxidation problem. The J-V curves in Fig. 6 were

Table 4. Obtained parameters using the CV technique of P3HT:Y6 thin film layers.

P3HT:Y6 blend wt%	Solid-state thin films				
	Eox (eV)	*Ered (eV)*	*E_{HOMO} (eV)*	*E_{LUMO} (eV)*	*Eg (eV)*
1:0	0.7	−1.6	−5.5	−3.2	2.3
1:0.6	0.8	−0.5	−5.5	−4.3	1.3
1:0.8	0.8	−0.5	−5.6	−4.3	1.3
1:1	0.6	−0.8	−5.4	−4.2	1.2
0.8:1	0.65	−0.6	−5.45	−4.2	1.25
0.6:1	0.68	−0.5	−5.48	−4.28	1.18
0.4:1	0.8	−0.4	−5.6	−4.24	1.36
0:1	0.9	−0.6	−5.7	−4.2	1.55

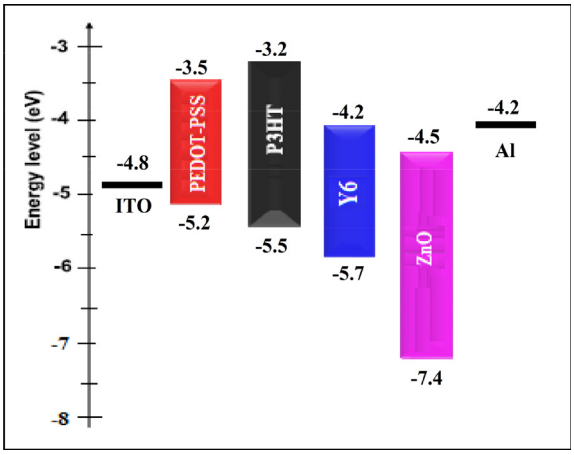

Fig. 5. Energy level diagram of the OPV layers.

obtained under illumination of 100 mW/cm^2 with a simulated AM 1.5G. Minimising energy loss is crucial to enhancing photovoltaic efficiency [35].

The total energy loss of a device can arise from radiative recombination loss, the energy loss from charge generation, and the energy loss from non-radiative recombination loss [36]. The voltage loss (V_{loss}) can be estimated according to the following equation [37]:

$$V_{loss} = Eg/q - V_{OC} \quad (5)$$

where q represents the elementary charge. A large voltage loss limited the improvement of the V_{OC} and PCE, as shown in Table 5. The average PCE values were determined by analysing four OPV devices fabricated for each weight ratio, and the numbers in brackets denote the maximum values of efficiency. The blend ratio of the donor and acceptor components can have an essential influence on

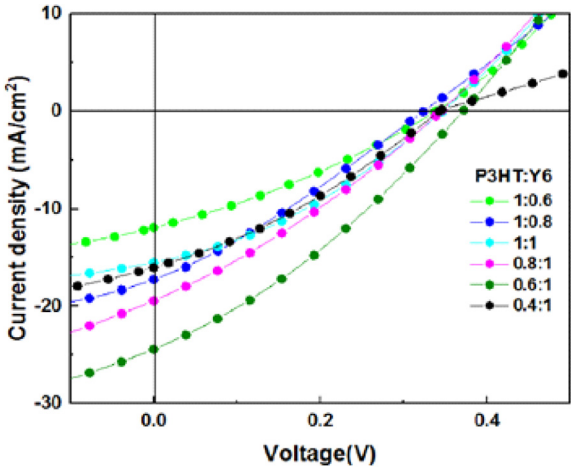

Fig. 6. J-V curves of OPV devices at different weight ratios.

Table 5. Electrical properties of the binary OPV devices.

P3HT:Y6 photoactive wt%	OPV devices						
	Voc (V)	*Jsc (mA/cm²)*	*FF %*	*Rs (Ω)*	*Rsh (Ω)*	*Ave. PCE %*	*V_{loss} (V)*
1:0.6	0.34	11.9	30.5	88	2705	1.105 ± 0.14 (1.21)	1.04
1:0.8	0.32	17.1	28.7	169	5866	1.57 ± 0.04 (1.6)	1.04
1:1	0.34	15.5	34.1	85	4867	1.81 ± 0.04 (1.84)	1.01
0.8:1	0.33	19.3	30.1	129	5470	1.94 ± 0.07 (1.99)	1.01
0.6:1	0.37	24.3	31.3	91	1367	2.29 ± 0.77 (2.84)	0.98
0.4:1	0.34	16.03	31.6	35	1085	1.705 ± 0.03 (1.73)	1.01

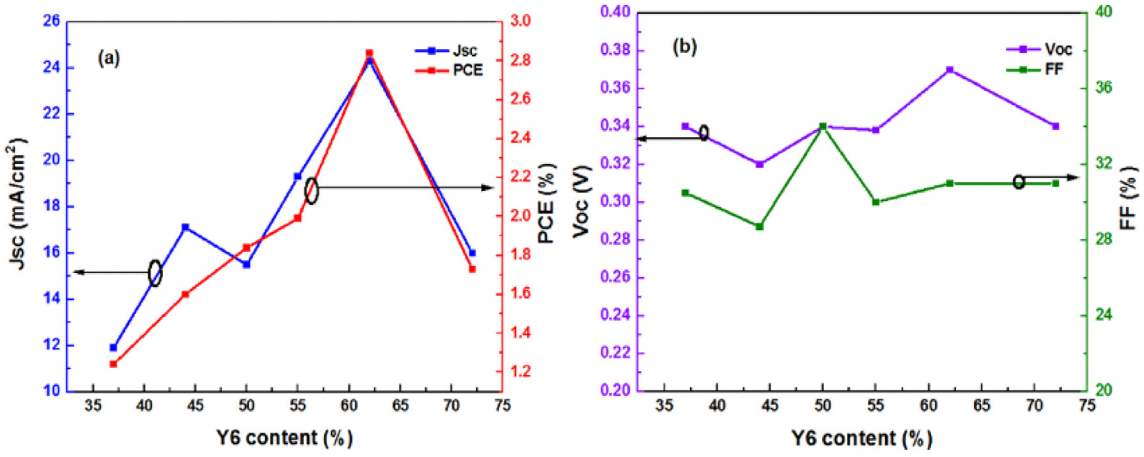

Fig. 7. Performance of P3HT:Y6 devices vs. the photoactive layer composition (a) short-circuit current density and power conversion efficiency; and (b) open-circuit voltage and fill factor.

photophysical properties. The results showed that enhancements made to Y6 content played a key role in boosting the overall performance of OPV devices. The best device performance with a PCE of 2.84% was achieved for a P3HT:Y6 (0.6:1) with a blend composition of about 62% Y6 by weight. The high values of J_{SC} and V_{OC} obtained were attributed to more charges extracted from the solar cells due to the efficient harvest of photons. With continuing to increase the content of the non-fullerene, the P3HT:Y6 devices with 72% Y6 (0.4:1) showed a drop in efficiency due to low J_{SC} and FF, as can be seen in Fig. 7. Lower P3HT crystallinity leads to poor exciton dissociation and unbalanced charge transport, resulting in poor transport and the extraction of free charges [38,39]. Despite the high aggregation organisation of P3HT chains and good FF, the P3HT:Y6 devices with 37% Y6 exhibited poor performance due to low Jsc values. Furthermore, the high values of shunt resistance and low values of series resistance contributed to an improvement in the FF factor by promoting strong molecular stacking during active layer formation and minimizing leakage current caused by defects. These effects ultimately enhance charge transport to the electrodes.

4. Conclusion

Absorption spectra analysis showed that Y6 exhibited a significant absorption capacity and efficient photon harvesting in the NIR spectrum region. Moreover, its energy levels were compatible with those of P3HT. As the Y6 content increased, the blend films exhibited low aggregation and low crystallinity, as evidenced by the results of the Raman and XRD tests. Notably, the Raman intensity positions at the primary C═C and C−C modes remained constant. This showed symmetrical broadening and low FWHM values, which showed that the materials used in the blend films were compatible. CV results suggest that the energy levels of the devices form a cascade alignment, which may be appropriate for exciton dissociation and charge transfer. Varying the blend ratio played a significant role in achieving results. The best performance was achieved at a ratio of 0.6:1 because of high photon harvesting in the polymer region.

Ethical statement

This manuscript does not contain any studies involving human subjects, human data, or human tissues.

Acknowledgements

The authors express their gratitude to Basra University for providing financial support. They also extend their thanks to their colleagues in the Nanotechnology Lab for their technical assistance with XRD, Raman, and photovoltaic tests. In terms of the author's contribution, Hassan Tarikhum B. was responsible for material synthesis and characterization, the fabrication and characterization of photovoltaics, and manuscript writing. Furqan Almyahi contributed to the structural designs of the devices and polymer structures, and Basil Ali contributed to the analysis of the results.

References

[1] B. Xiao, A. Tang, J. Zhang, A. Mahmood, Z. Wei, E. Zhou, Achievement of high voc of 1.02 V for P3HT-based organic solar cell using a benzotriazole-containing non-fullerene acceptor, Adv. Energy Mater. 7 (2017) 1–7, https://doi.org/10.1002/aenm.201602269.

[2] B. Xiao, A. Tang, L. Cheng, J. Zhang, Z. Wei, Q. Zeng, E. Zhou, Non-fullerene acceptors with A2 = A1-D-A1 = A2 skeleton containing benzothiadiazole and thiazolidine-2,4-dione for high-performance P3HT-based organic solar cells, Sol. RRL 1 (2017) 1–10, https://doi.org/10.1002/solr.201700166.

[3] F. Liu, J. Zhang, Z. Zhou, J. Zhang, Z. Wei, X. Zhu, Poly(3-hexylthiophene)-Based non-fullerene solar cells achieve high photovoltaic performance with small energy loss, J. Mater. Chem. A 5 (2017) 16573–16579, https://doi.org/10.1039/C7TA05108E.

[4] Y.W. Su, Y.C. Lin, K.H. Wei, Evolving molecular architectures of donor-acceptor conjugated polymers for photovoltaic applications: from one-dimensional to branched to two-dimensional structures, J. Mater. Chem. A 5 (2017) 24051–24075, https://doi.org/10.1039/c7ta07228g.

[5] Y.-W. Su, Y.-S. Huang, H.-C. Huang, P.-T. Chen, Optoelectronic properties of a benzodithiophene-based organic photovoltaic, ECS J. Solid State Sci. Technol. 10 (2021) 075003, https://doi.org/10.1149/2162-8777/ac12b4.

[6] B. Xiao, A. Tang, J. Yang, Z. Wei, E. Zhou, P3HT-Based photovoltaic cells with a high voc of 1.22 V by using a benzotriazole-containing nonfullerene acceptor end-capped with thiazolidine -2,4-dione, ACS Macro Lett. 6 (2017) 410–414, https://doi.org/10.1021/acsmacrolett.7b00097.

[7] X. Wang, A. Tang, J. Yang, M. Du, J. Li, G. Li, Q. Guo, E. Zhou, Tuning the intermolecular interaction of A2-A1-D-A1-A2 type non-fullerene acceptors by substituent engineering for organic solar cells with ultrahigh V OC of ~1.2 V, Sci. China Chem. 63 (2020) 1666–1674, https://doi.org/10.1007/s11426-02 0-9840-x.

[8] B. Fan, Z. Zeng, W. Zhong, L. Ying, D. Zhang, M. Li, F. Peng, N. Li, F. Huang, Y. Cao, Optimizing microstructure morphology and reducing electronic losses in 1 cm2 polymer solar cells to achieve efficiency over 15, ACS Energy Lett. 4 (2019) 2466–2472, https://doi.org/10.1021/acsenergylett.9b01447.

[9] B. Fan, M. Li, D. Zhang, W. Zhong, L. Ying, Z. Zeng, K. An, Z. Huang, L. Shi, G.C. Bazan, G.C. Bazan, F. Huang, Y. Cao, Tailoring regioisomeric structures of π-conjugated polymers containing monofluorinated π-bridges for highly efficient polymer solar cells, ACS Energy Lett. 5 (2020) 2087–2094, https://doi.org/10.1021/acsenergylett.0c00939.

[10] J. Xiong, K. Jin, Y. Jiang, J. Qin, T. Wang, J. Liu, Q. Liu, H. Peng, X. Li, A. Sun, X. Meng, L. Zhang, L. Liu, W. Li, Z. Fang, X. Jia, Z. Xiao, Y. Feng, X. Zhang, K. Sun, S. Yang, S. Shi, L. Ding, Thiolactone copolymer donor gifts organic solar cells a 16.72% efficiency, Sci. Bull. 64 (2019) 1573–1576, https://doi.org/10.1016/j.scib.2019.10.002.

[11] Q. Liu, Y. Jiang, K. Jin, J. Qin, J. Xu, W. Li, J. Xiong, J. Liu, Z. Xiao, K. Sun, S. Yang, X. Zhang, L. Ding, 18% efficiency organic solar cells, Sci. Bull. 65 (2020) 272–275, https://doi.org/10.1016/j.scib.2020.01.001.

[12] J. Yang, Y. Geng, J. Li, B. Zhao, Q. Guo, E. Zhou, A-DA′D-A-Type non-fullerene acceptors containing a fused heptacyclic ring for poly(3-hexylthiophene) -based polymer solar cells, J. Phys. Chem. C 124 (2020) 24616–24623, https://doi.org/10.1021/acs.jpcc.0c07162.

[13] N.A. Cooling, E.F. Barnes, F. Almyahi, K. Feron, M.F. Al-Mudhaffer, A. Al-Ahmad, B. Vaughan, T.R. Andersen, M.J. Griffith, A.S. Hart, A.G. Lyons, W.J. Belcher, P.C. Dastoor, A low-cost mixed fullerene acceptor blend for printed electronics, J. Mater. Chem. A 4 (2016) 10274–10281, https://doi.org/10.1039/c6ta04191d.

[14] F. Almyahi, T.R. Andersen, A. Fahy, M. Dickinson, K. Feron, W.J. Belcher, P.C. Dastoor, The role of surface energy control in organic photovoltaics based on solar paints, J. Mater. Chem. A 7 (2019) 9202–9214, https://doi.org/10.1039/c8ta09521c.

[15] K. Anagnostou, M.M. Stylianakis, K. Petridis, E. Kymakis, Building an organic solar cell: fundamental procedures for device fabrication, Energies 12 (2019) 2188, https://doi.org/10.3390/en12112188.

[16] Y. Lin, J. Wang, Z.G. Zhang, H. Bai, Y. Li, D. Zhu, X. Zhan, An electron acceptor challenging fullerenes for efficient polymer solar cells, Adv. Mater. 27 (2015) 1170–1174, https://doi.org/10.1002/adma.201404317.

[17] J. Yuan, Y. Zhang, L. Zhou, G. Zhang, H.-L. Yip, T.-K. Lau, X. Lu, C. Zhu, H. Peng, P.A. Johnson, M. Leclerc, Y. Cao, J. Ulanski, Y. Li, Y. Zou, Single-junction organic solar cell with over 15% efficiency using fused-ring acceptor with electron-deficient core, Joule 3 (2019) 1140–1151, https://doi.org/10.1016/j.joule.2019.01.004.

[18] C. Hellmann, F. Paquin, N.D. Treat, A. Bruno, L.X. Reynolds, S.A. Haque, P.N. Stavrinou, C. Silva, N. Stingelin, Controlling the interaction of light with polymer semiconductors, Adv. Mater. 25 (2013) 4906–4911, https://doi.org/10.1002/adma.201300881.

[19] O.P. Dimitriev, Effect of confinement on photophysical properties of P3HT chains in PMMA matrix, Nanoscale Res. Lett. 12 (2017) 510, https://doi.org/10.1186/s11671-017-2270-y.

[20] B.H. Jiang, C.P. Chen, H. Te Liang, R.J. Jeng, W.C. Chien, Y.Y. Yu, The role of Y6 as the third component in fullerene-free ternary organic photovoltaics, Dyes Pigments 181 (2020) 108613, https://doi.org/10.1016/j.dyepig.2020.108613.

[21] N. Banerji, S. Cowan, E. Vauthey, A.J. Heeger, Ultrafast relaxation of the poly(3-hexylthiophene) emission spectrum, J. Phys. Chem. C 115 (2011) 9726–9739, https://doi.org/10.1021/jp1119348.

[22] Z.A. Alrowaili, M. Ezzeldien, M.I. Mohammed, I.S. Yahia, Design of a low-cost laser CUT-OFF filters using carmine dye-doped PVA polymeric composite films, Results Phys. 18 (2020) 103203, https://doi.org/10.1016/j.rinp.2020.103203.

[23] N. Sangiorgi, L. Aversa, R. Tatti, R. Verucchi, A. Sanson, Spectrophotometric method for optical band gap and electronic transitions determination of semiconductor materials, Opt. Mater. (Amst). 64 (2017) 18–25, https://doi.org/10.1016/j.optmat.2016.11.0141.

[24] N. Chandrasekaran, A. Kumar, L. Thomsen, D. Kabra, C.R. McNeill, High performance as-cast P3HT: PCBM devices: understanding the role of molecular weight in high regioregularity P3HT, Mater. Adv. 2 (2021) 2045–2054, https://doi.org/10.1039/d0ma00738b.

[25] L. Wu, S. Casado, B. Romero, J.M. Otón, J. Morgado, C. Müller, R. Xia, J. Cabanillas-Gonzalez, Ground state host-guest interactions upon effective dispersion of regioregular poly(3-hexylthiophene) in poly(9,9-dioctylfluorene-alt-benzothiadiazole), Macromolecules 48 (2015) 8765–8772, https://doi.org/10.1021/acs.macromol.5b02111.

[26] Y. Gao, J.K. Grey, Resonance chemical imaging of polythiophene/fullerene photovoltaic thin films: mapping morphology-dependent aggregated and unaggregated C=C species, J. Am. Chem. Soc. 131 (2009) 9654–9662, https://doi.org/10.1021/ja900636z.
[27] S. Falke, P. Eravuchira, A. Materny, C. Lienau, Raman spectroscopic identification of fullerene inclusions in polymer/fullerene blends, J. Raman Spectrosc. 42 (2011) 1897–1900, https://doi.org/10.1002/jrs.2966.
[28] Y.S. Kim, Y. Lee, J.K. Kim, E.O. Seo, E.W. Lee, W. Lee, S.H. Han, S.H. Lee, Effect of solvents on the performance and morphology of polymer photovoltaic devices, Curr. Appl. Phys. 10 (2010) 985–989, https://doi.org/10.1016/j.cap.2009.10.013.
[29] D.E. Motaung, G.F. Malgas, C.J. Arendse, S.E. Mavundla, C.J. Oliphant, D. Knoesen, The influence of thermal annealing on the morphology and structural properties of a conjugated polymer in blends with an organic acceptor material, J. Mater. Sci. 44 (2009) 3192–3197, https://doi.org/10.1007/s 10853-009-3425-8.
[30] F. Liu, D. Chen, C. Wang, K. Luo, W. Gu, A.L. Briseno, J.W.P. Hsu, T.P. Russell, Molecular weight dependence of the morphology in P3HT:PCBM solar cells, ACS Appl. Mater. Interfaces 6 (2014) 19876–19887, https://doi.org/10.1021/am505283k.
[31] B. Xiao, M. Du, X. Wang, Z. Xiao, G. Li, A. Tang, L. Ding, Y. Geng, X. Sun, E. Zhou, Effects of oxygen atoms introduced at different positions of non-fullerene acceptors in the performance of organic solar cells with poly(3-hexylthiophene), ACS Appl. Mater. Interfaces 12 (2020) 1094–1102, https://doi.org/10.1021/acsami.9b16662.
[32] S. Wilken, D. Scheunemann, V. Wilkens, J. Parisi, H. Borchert, Improvement of ITO-free inverted polymer-based solar cells by using colloidal zinc oxide nanocrystals as electron-selective buffer layer, Org. Electron. 13 (2012) 2386–2394, https://doi.org/10.1016/j.orgel.2012.07.026.
[33] T. Jiemsakul, K. Jiramitmongkon, U. Asawapirom, C. Chotsuwan, Investigation of P3HT electrochromic polymer films prepared by ultrasonication of polymer solutions, J. Mater. Sci. 52 (2017) 8485–8492, https://doi.org/10.1007/s10853-017-1109-3.
[34] B.K. Sharma, N. Khare, S. Ahmad, A ZnO/PEDOT:PSS based inorganic/organic hetrojunction, Solid State Commun. 149 (2009) 771–774, https://doi.org/10.1016/j.ssc.2009.02.035.
[35] J. Wang, H. Yao, Y. Xu, L. Ma, J. Hou, Recent progress in reducing voltage loss in organic photovoltaic cells, Mater. Chem. Front. 5 (2021) 709–722, https://doi.org/10.1039/d0qm00581a.
[36] B.H. Jiang, Y.P. Wang, Y.W. Su, J.F. Chang, C.C. Chueh, M.H. Shen, T.S. Shieh, R.J. Jeng, C.P. Chen, Realizing stable high-performance and low-energy-loss ternary photovoltaics through judicious selection of the third component, Sol. RRL 5 (2021) 1–11, https://doi.org/10.1002/solr.202 100450.
[37] N. Wang, W. Yang, S. Li, M. Shi, T.K. Lau, X. Lu, R. Shikler, C.Z. Li, H. Chen, A non-fullerene acceptor enables efficient P3HT-based organic solar cells with small voltage loss and thickness insensitivity, Chinese Chem. Lett. 30 (2019) 1277–1281, https://doi.org/10.1016/j.cclet.2019.01.010.
[38] S.S. Van Bavel, M. Bärenklau, G. De With, H. Hoppe, J. Loos, P3HT/PCBM bulk heterojunction solar cells: impact of blend composition and 3D morphology on device performance, Adv. Funct. Mater. 20 (2010) 1458–1463, https://doi.org/10.1002/adfm.200902247.
[39] J.A. Renz, T. Keller, M. Schneider, S. Shokhovets, K.D. Jandt, G. Gobsch, H. Hoppe, Solar energy materials & solar cells multiparametric optimization of polymer solar cells, A Route to Reproducible High Efficiency 93 (2009) 508–513, https://doi.org/10.1016/j.solmat.2008.11.001.